A Joint Numerical-Experimental Study on Impact Induced Intra-laminar and Inter-laminar Damage in Laminated Composites

Appl Compos Mater (2016) 23:219–237
DOI 10.1007/s10443-015-9457-0

A Joint Numerical-Experimental Study on Impact Induced Intra-laminar and Inter-laminar Damage in Laminated Composites

A. Riccio[1] **· F. Caputo**[1] **· G. Di Felice**[1] **· S. Saputo**[1] **·**
C. Toscano[2] **· V. Lopresto**[3]

Received: 25 June 2015 / Accepted: 7 July 2015 / Published online: 29 July 2015

Abstract The investigation of the mechanical response of fibre-reinforced composite laminates under impact loads can be very difficult due to the occurrence of simultaneous failure phenomena. Indeed, as a consequence of low velocity impacts, intra-laminar damages, like fibre and matrix cracking, and inter-laminar damages, such as delaminations, can take place simultaneously. These damage mechanisms can lead to significant reductions in strength and stability of the composite structure. In this paper a joint numerical-experimental study is proposed which, by means of non-destructive testing techniques (Ultra-sound and thermography) and non-linear explicit FEM analyses, aims to completely characterise the impact induced damage in composite laminates under low velocity impacts. Indeed the proposed numerical tool has been used to improve the understanding of the experimental data obtained by Non-Destructive Techniques. Applications on samples tested according to the AECMA (European Association of Aerospace Manufacturers) prEn6038 standard at three different impact energies are presented. The interaction between numerical and experimental investigation allowed to obtain an exhaustive insight on the different phases of the impact event considering the inter-laminar damage formation and evolution.

Keywords Laminate · Impact behaviour · Finite element analysis (FEA) · Damage mechanics · Non-destructive testing

✉ A. Riccio
aniello.riccio@unina2.it

[1] Department of Industrial and Information Engineering, Second University of Naples, via Roma 29, 81031 Aversa, Italy

[2] C.I.R.A. Italian Aerospace Research Centre, via Maiorise S.N., 81043 Capua, Italy

[3] Department of Material Engineering, University of Naples "FEDERICO II", Naples, Italy

1 Introduction

The increasing use of fibre-reinforced composite laminates in several industrial sectors (automotive, aerospace, Naval and railways) encouraged by their low weight, excellent strength and excellent stiffness properties, requires a deep knowledge on the composite's mechanical behaviour. However, these outstanding materials have shown poor damage resistance performances when subjected to impact events [1, 2]. A classification of impacts events on composites can be attempt based on the impact cinematic variables [1]. Indeed a relevant difference exists, in terms of damage formation and evolution in composites between low and high velocity impacts. Differently from high velocity impacts, where the damage is generated in the proximity of the contact area and then transmitted through the thickness [3, 4] in a limited area nearby the impact location, in low velocity impacts the most of the damage formation takes place not necessarily close to the impact surface and it can extend to a very large area [5–7], compromising the residual bearing capability of the structural components. Hence low velocity impact events can be considered of relevant interest when dealing with the structural integrity of composite components. The damage caused by these events is a mixture of several failure modes such as matrix cracking, fiber breakage and delamination [5, 6]. In particular, low velocity impact induced delaminations have been found to seriously degrade the strength and the integrity of the whole structures [7, 8] propagating during service and leading to the collapse of the structure. The prediction of the impact response and, in particular, of the induced delaminations in composite laminates under low velocity impacts, has been widely treated in literature leading to the definition of analytical, experimental and numerical approaches [9–15] aimed to optimize the damage tolerance in composite structures.

The complex physical phenomena involved in the impact events make the analytical approaches suitable just for particular and very specific applications (for the most for very simple geometries and boundary conditions) [9]. On the other hand, a comprehensive completely empirical study for the impact induced damage prediction in composite structures is precluded by the technical difficulties and by the high costs involved in ad-hoc experimental campaigns [12–20].

Hence, in the most general cases, numerical predictive models taking into account several dynamics related aspects and implying the use of specific contact formulations, stress based failure modes, material degradation rules and fracture mechanics [16, 17] should be used.

In literature a large number of predictive methods to model initiation and growth of impact induced damage in laminates can be found [21–26]. The stress-based continuum damage mechanics [5, 6] has been found not particularly suitable to model discrete failure phenomena characterized by highly localized stresses at geometrical or material discontinuities such as the inter-laminar discontinuities [26–29] while fracture mechanics is, in general, widely adopted to analyze the progression of inter-laminar cracks by means of FE-based procedures such as the Virtual Crack Closure technique (VCCT) or cohesive zone models (CZM) [21, 26, 30, 31]. The VCCT requires the assumption of a pre-existing crack and the application of adaptive re-meshing rules in order to adjust the mesh according to the evolving delamination front. Furthermore, the VCCT has been found sensitive to mesh and time-increments, hence a trial-error procedure (changing mesh size and time-increments) is required to fit experimental and numerical results [29, 32, 33]. On the other hand, the CZM, combining strength-based criteria to predict damage initiation and fracture mechanics energy criteria to simulate damage propagation, can guarantee good results for the simulation of discrete failure models [34], without the limitations or with less limitations with respect to VCCT. It is possible to find

many contributions in literature [35–37] where cohesive elements are placed at the neighbouring plies interfaces to model delaminations occurring in composite laminates under low-velocity impact events.

The combined effect of impact induced intra-laminar [38] and inter-laminar damages has been investigated by various authors adopting either cohesive [39–42] or special spring elements [43, 44] to model delaminations at the interfaces between layers and major matrix cracks developing in impacted laminates.

Both inter-laminar and intra-laminar predictions have been found affected by mesh sensitivity problems. The mesh size dependence problem, limiting the crack propagation effectiveness and invalidating the results in terms of inter-laminar damage, has been outlined in [45] while the problems of mesh dependence related to the intra-laminar damage prediction have been introduced in [46–51] where a number of methodologies, based on energy criteria, are used to simulate intra-laminar damage in composite laminates by instantaneous material degradation rules. Alternative mesh-insensitive damage models based on CDM have been demonstrated to allow the simulation of intra-laminar damage onset and growth by introducing gradual degradation factors of material mechanical properties [52].

Several authors studied the behavior of impacted laminates with different stacking sequences [53] using a CDM approach (to simulate fiber and matrix failure initiation and propagation) and CZM (to simulate the detachment of the plies) during impacts phenomena. This combination of numerical methodologies has been found effective providing a good numerical-experimental correlation in terms of force time history, general damage and failure envelope in [15, 54] for different impact energies value. In particular, in [54], the experimental shape and dimension of inter-laminar damage was obtained using fluorescent penetrant techniques. This experimental data was relevant to check the quality of numerical results in terms of inter-laminar damage size and orientation.

Similar numerical models have been adopted in [55, 56] and again comparisons with experimental data in terms of inter-laminar damage extension are provided. However only the size of the global inter-laminar damage over the laminated thickness is provided without any indication about the inter-laminar damage distribution over the different ply interfaces of the laminate. The same consideration extends to [41, 43, 54]. The lack of numerical-experimental exhaustive (quantitatively and qualitatively) correlation does not allow to completely validate the proposed complex numerical models and to assess the effectiveness of these models.

Hence, despite of the research effort spent in the last decades, further numerical-experimental correlations, using alternative, effective and concurrent experimental techniques, are envisaged to increase the understanding of the involved physical phenomena and to improve the effectiveness of the design tools.

The purpose of this paper is to investigate the inter-laminar damage induced by low velocity impacts on laminated composites by means of a combined Numerical-Experimental methodology. The numerical simulation model based on the combined use of CDM and CZM to capture the shape, size and position of inter-laminar and intra-laminar damage was implemented in the explicit FEM code ABAQUS. Indeed, the introduction of techniques for the simulation of the intra-laminar damage onset and evolution in the proposed numerical model has allowed to take into account, from a numerical point of view, the influence of intra-laminar damage on the inter-laminar damage formation and evolution.

Thermography, Ultrasound A-scan and Ultrasound C-Scan have been used to determine the inter-laminar damage status after impact in composite plates tested according to the AECMA

(European Association of Aerospace Manufacturers) prEn6038 standard for three different impact energies.

The combination of the Numerical model and experimental NDT techniques has been found very effective for the characterization of the impact induced inter-laminar damage for the laminated composite plates under investigation.

In the presented work the correlation between numerical results and experimental data from different independent experimental sources, in terms of shape and dimensions of delaminations, has been demonstrated to be able to improve the understanding of the physical phenomena behind the low velocity impact events for the laminated plates under consideration and to cross-validate the proposed numerical model for future applications.

In section 2 the experimental procedures adopted to perform the impact and the Non-Destructive tests are described in detail while in section 3 information on the numerical model are provided. Finally in section 4 the NDT experimental data and the numerical results are correlated and discussed.

2 Experimental Tests Results

2.1 Impact Test

The investigated specimens have been manufactured and impact tested according to the European association of Aerospace Manufacturers (AECMA) standard prEN 6038 . The drop test under low velocity impact has been realized with a drop tower system. Three different test types with three different energy values have been performed (the three energy values have been obtained by changing the height h and hence the velocity v_0 values of the impactor). Rectangular flat specimens (150 mm×100 mm), placed on a flat support fixture with a 125 mm×75 mm rectangular cut-out, have been impacted by an hemispherical (Radius= 8 mm) impactor with mass m=3.64 kg. A symmetric balanced layup ($[0/90/45/-45]_s$) has been considered for the impacted specimens made of G1157\RTM-6 carbon- epoxy unidirectional pre-preg plies (0.3 mm thick). During the impact event, the impact energy transferred by a body of mass m and initial velocity v_0 to the composite plate can be evaluated as:

$$E_i = \frac{mv_0^2}{2} \tag{1}$$

Besides, the kinetic energy $KE_{(t)}$ of the specimen at time t can be expressed by:

$$KE(t) = \frac{mV_0^2}{2} - \frac{m(V_i(t))^2}{2} \tag{2}$$

Where $V_i(t)$ is the impactor velocity at time t obtained as

$$V_i(t) = V_0 - \frac{1}{m}\int_0^t F_{exp}\,dt \tag{3}$$

being F_{exp} the reaction force of the specimen during the impact event. The kinetic energy transferred at time t to the composite plate can be written as:

$$KE(t) = E_e + E_a \tag{4}$$

where E_a and E_e are respectively the absorbed energy for damage formation and the elastic deformation energy. Obviously the rate of absorbed energy depends on the active failure mechanisms which are strictly related to impactor mass and velocity, impactor shape, structure shape, fiber and matrix type and stacking sequence.

2.2 Thermography Non-Destructive Tests

After being impacted, the panels have been non-destructively inspected. Initially, an infrared thermography lock-in test has been performed by heating up the specimen by a modulated light and by acquiring the surface temperature variations by a thermal camera. The thermal energy delivered into the material propagates as thermal waves within it, being partially reflected. The reflected waves interfere with the incoming ones, producing an oscillating interference pattern which can be measured in terms of amplitude (representative of the amount of thermal energy transmitted to the material) and phase (phase delay between the delivered and reflected thermal waves). The application of this method is based on the use of simple relations among the thermal diffusion length μ, the thermal diffusivity coefficient α and the wave frequency $f = \omega/2\pi$, such as:

$$\mu = \sqrt{\frac{\alpha}{\pi f}} \tag{5}$$

Indeed, the thermal diffusion length μ, is representative of the maximum depth at which effective amplitude images can be taken. On the other hand, effective phase images (representative of the homogeneity status and, eventually, of the defects depth) can be taken up to about double the thermal diffusion length. The following relation providing the maximum depth at which effective phase images can be taken, holds:

$$p = 1.8\mu \tag{6}$$

Since the frequency has been selected providing p to be equal to the thickness of the composite panel L, the thermal diffusivity of the panel has been obtained, from Eqs. (5) to (6), as:

$$\alpha = \pi f \left(\frac{L}{1.8}\right)^2 \tag{7}$$

By this approach, the depth of defects, embedded in CFRP panels, can be also evaluated, once the diffusivity is known, simply by tuning f. The adopted lock-in procedure allowed to detect the impact damage (located at different depth of the specimen) and to measure its dimensions.

2.3 Ultrasound A-SCAN and C-SCAN Non-Destructive Tests

The impacted panels have been also non-destructively inspected by means of Ultra-Sonic tests. In this work, the Pulse Echo technique, characterized by an emitting probe capturing the echo signals to identify the damage inside the specimen, has been used. The C-scan and A-scan formats have been used to collect and display the Ultrasonic data. The C-scan representation provides a plan-type view of the location and size of test specimen features. The plane of the image is parallel to the scan pattern of the transducer. The C-scan representation has been

produced with the Olympus OmniScan® SX Phased array automated data acquisition system by means of the a16:64PR phased array unit. The A-Scan Presentation displays the amount of received ultrasonic energy as a function of time obtained by the BondMasterTM 1000 (Staveley Instruments) composite tester in Resonance mode. According to the BondMasterTM 1000 testing methodology, when the probe is located over a damaged section, the dot on the screen instrument (indicating the amplitude and the phase of the sweep) moves outer of the no-damage box, previously defined during the calibration procedure performed over a not damaged area. In Fig. 1 the classification of the flaw entity is schematically provided as a function of the dot position with respect to the bounding box identifying the undamaged status. Referring to Fig. 1a, A is representative of the measurement in an undamaged zone, B is representative of a limit area (where the flaw is partial), while C is representative of a measurement over a fully damaged area. In order to provide a representation of the damaged area in the laminate plane, the samples have been prepared drawing an equally spaced grid over the impacted surface (see Fig. 1b). According to the probe dimension (S-PR-5: 250 kHz, 9.525 mm diameter), a 10 mm spaced grid has been chosen. The results (undamaged, partially damaged, fully damaged) obtained for each point of the grid have been stored and graphically represented in the laminate plane as shown in Fig. 1c (the red color is associated to the damaged area).

3 Numerical Modelling

In the frame of the present study, in order to fully appreciate the low velocity impact induced delamination onset and evolution at ply level, finite element analyses have been used. An advanced finite element model has been introduced to predict the occurring simultaneous inter-laminar and intra-laminar failure mechanisms in the impacted composite plates for all the three investigated impact energy levels. The Abaqus-Explicit FE code has been used [57] as platform to implement the numerical model using a combination of cohesive elements (COH3D8) and continuum shell elements (SC8R). Each ply is modelled with 8 nodes elements with 3° of freedom for each node and a reduced integration scheme. The mesh-insensitive damage models described in [52] and based on a smeared crack approach allowing

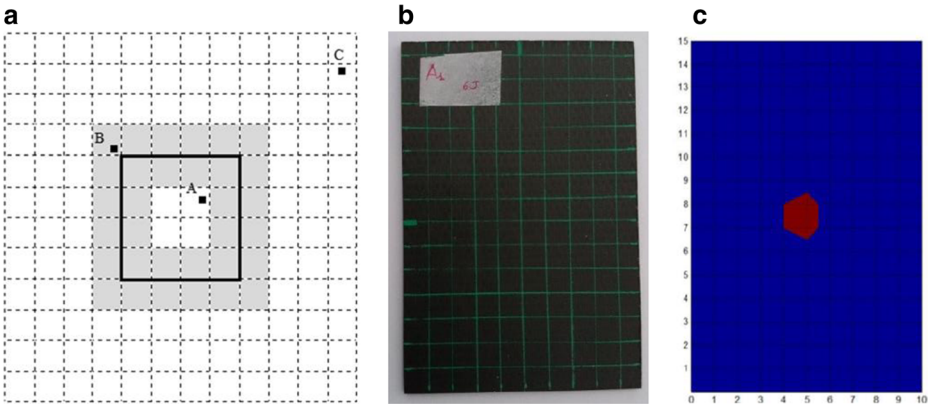

Fig. 1 **a** Definition of bounding box and dot classification; **b** Grid drawn on the sample; **c** Example of contour plot of the damage for the inspected samples

to evaluate the fracture energy over the elements volume has been adopted for the proposed numerical formulation.

3.1 Intra-laminar Damage Modelling

The intra-laminar failure mechanisms have been simulated by using the Hashin's failure criteria [58, 59] together with a Continuum Damage Mechanics approach taking into account the degradation of material properties occurring as a consequence of damage onset and evolution. Hashin's criteria allow to distinguish among different intra-laminar failure modes:

$$\text{Fiber tension} = \left(\hat{\sigma}_{11} \geq 0\right) \quad F_{ft} = \left(\frac{\hat{\sigma}_{11}}{X^T}\right)^2 + \left(\frac{\hat{\sigma}_{12}}{S^L}\right)^2 = 1 \tag{8}$$

$$\text{Fiber compression} = \left(\hat{\sigma}_{11} < 0\right) \quad F_{fc} = \left(\frac{\hat{\sigma}_{11}}{X^C}\right)^2 = 1 \tag{9}$$

$$\text{Matrix Tension} = \left(\hat{\sigma}_{22} \geq 0\right) \quad F_{mt} = \left(\frac{\hat{\sigma}_{22}}{Y^T}\right)^2 + \left(\frac{\hat{\sigma}_{12}}{S^L}\right)^2 = 1 \tag{10}$$

$$\text{Matrix Compression} = \left(\hat{\sigma}_{22} < 0\right) \quad F_{mc} = \left(\frac{\hat{\sigma}_{22}}{2S^T}\right)^2 + \left[\left(\frac{Y^C}{2S^T}\right)^2 - 1\right]\frac{\hat{\sigma}_{22}}{Y^C} + \left(\frac{\hat{\sigma}_{12}}{S^L}\right)^2 = 1 \tag{11}$$

The relation adopted for each intra-laminar failure mode is graphically shown in Fig. 2a.

It should be emphasized that the adopted model takes into account fibre breakage and matrix cracking while the intra-laminar matrix macro-cracks and splitting associated to delaminations formation are not considered in order to limit the computational cost associated to the numerical analyses. However, as demonstrated by the numerical-experimental correlation presented in the next section, this limitation in the numerical model seemed to have a very partial influence, for the analysed composite plates, on the accuracy of numerical results in terms of inter-laminar damage onset and evolution, which was the main focus of the paper.

According to Fig. 2a, an initialization (undamaged) phase and a propagation (damaged) phase can be distinguished. When the stress exceeds the limit value σ^0_{eq} (satisfaction of a specific Hashin intra-laminar failure criterion), the element is considered partially damaged and the damage propagation phase starts (point A). Once a damage initiation criterion is satisfied, further loading causes a progressive degradation of the material stiffness coefficients, controlled by the damage variable d_I for each failure mode I:

$$d_I = \frac{\delta^t_{I,eq}\left(\delta_{I,eq} - \delta^0_{I,eq}\right)}{\delta_{I,eq}\left(\delta^t_{I,eq} - \delta^0_{I,eq}\right)} \quad ; \quad \left(\delta^0_{I,eq} \leq \delta_{I,eq} \leq \delta^t_{I,eq}\right) \quad \text{I} \in (f_c, f_t, m_c, m_t) \tag{12}$$

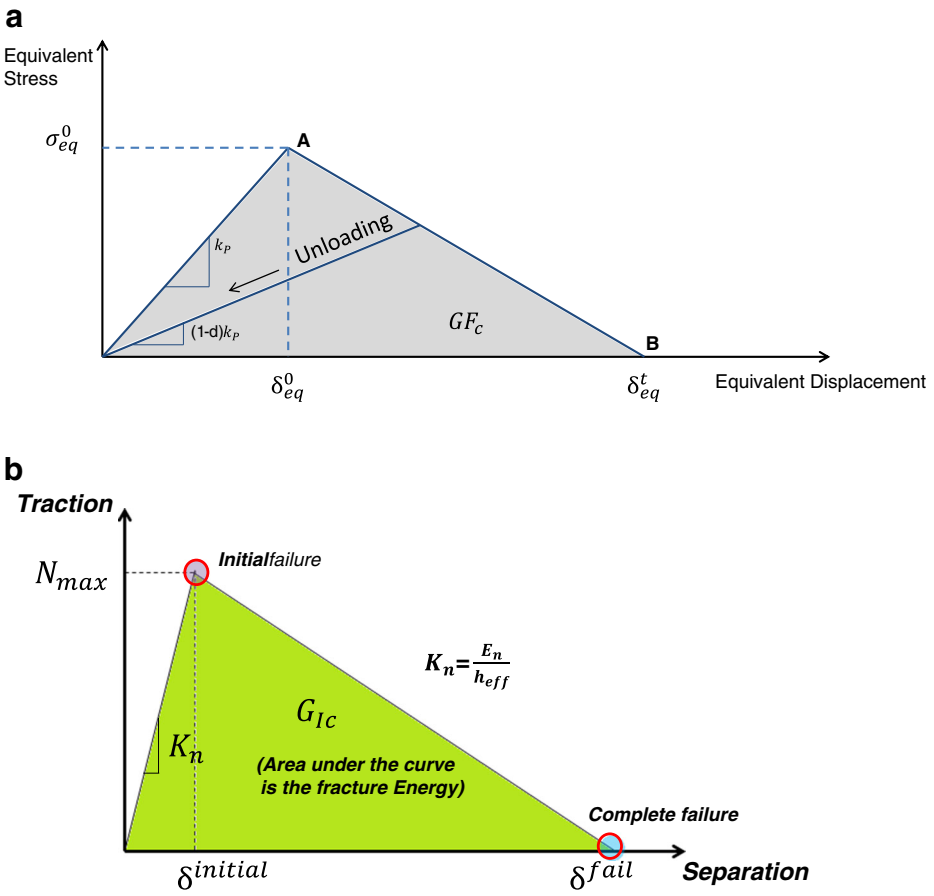

Fig. 2 **a** Constitutive relation adopted for each intra-laminar failure mode; **b** Traction-separation law for cohesive material

In Eq. (12) $\delta_{I,eq}^0$ is the equivalent displacement at which the specific Hashin's criterion is satisfied, and $\delta_{I,eq}^t$ is the equivalent displacement at which the material is completely damaged ($d_I = 1$). In Eq. (12) $\delta_{I,eq}^t$ is not known but it can be computed from the following relation, assuming that the fracture energy GF_{Ic} is specified and the softening is linear:

$$\delta_{I,eq}^t = \frac{2\left(GF_{Ic} - \frac{\sigma_{I,eq}^0 \delta_{I,eq}^0}{2}\right)}{\sigma_{I,eq}^0} \tag{13}$$

The evolution law of the damage variable in the post-damage initiation phase, as a generalization of the approach presented in [60], is based on the fracture energy dissipated during the damage process, GFIc.

In the Table 1 are reported the value of equivalent displacement and stress for the four damage modes. ‹› is Macauley bracket operator, defined for each $\gamma \in$ as:

$$\langle \gamma \rangle = \frac{(\gamma + |\gamma|)}{2}. \tag{14}$$

Table 1 Equivalent displacement and stress definition

Failure mode		δ_{eq}	σ_{eq}
Fiber tension	$(\hat{\sigma}_{11} \geq 0)$	$L_c\sqrt{\langle\varepsilon_{11}\rangle^2 + \alpha\varepsilon_{12}{}^2}$	$\frac{L_c(\langle\sigma_{11}\rangle\langle\varepsilon_{11}\rangle + \alpha\sigma_{12}\varepsilon_{12})}{\delta_{eq}^{ft}}$
Fiber compression	$(\hat{\sigma}_{11} \leq 0)$	$L_c\langle-\varepsilon_{11}\rangle$	$L_c\langle-\sigma_{11}\rangle\ \frac{\langle\varepsilon_{11}\rangle}{\delta_{eq}^{fc}}$
Matrix tension	$(\hat{\sigma}_{22} \geq 0)$	$L_c\sqrt{\langle\varepsilon_{22}\rangle^2 + \varepsilon_{12}{}^2}$	$\frac{L_c(\langle\sigma_{22}\rangle\langle\varepsilon_{22}\rangle + \sigma_{12}\varepsilon_{12})}{\delta_{eq}^{mt}}$
Matrix compression	$(\hat{\sigma}_{22} \leq 0)$	$L_c\sqrt{\langle-\varepsilon_{22}\rangle^2 + \varepsilon_{12}{}^2}$	$L_c(\langle-\sigma_{22}\rangle\ \langle-\varepsilon_{22}\rangle\ \frac{+\sigma_{12}\varepsilon_{12})}{\delta_{eq}^{mt}}$

In order to reduce the mesh dependency during the damage initiation and material softening phases a characteristic length, L_c, has been introduced. A number of methods are suggested for computing the characteristic length. Bazant and Oh [61, 62] proposed the following relation for square elements to be applied at each integration point of the element:

$$L_c = \frac{\sqrt{A_{ip}}}{cos\theta} \quad |\theta| \leq 45^\circ \tag{15}$$

Where A_{ip} is the area associated to an integration point i and θ is the angle between the mesh line along which the crack band advances and the crack direction. This method has been shown to be computationally efficient and to work reasonably well [63].

3.2 Inter-laminar Damage Modelling

Cohesive zone model (CZM) based elements have been adopted in order to simulate the inter-laminar damage formation ad evolution in the impacted composite plates. The cohesive behaviour is defined by a traction-separation law based on the Strain Energy Release Rate. The constitutive response in cohesive elements is characterized by an initial damage phase and a damage evolution phase, as schematically shown for peel fracture mode in Fig. 2b.

The failure criterion used for the definition of the damage initiation (first phase of the traction-separation law) for the cohesive elements is the quadratic nominal stress criterion (QUADS):

$$\left(\frac{\sigma_n}{N_{max}}\right)^2 + \left(\frac{\sigma_t}{T_{max}}\right)^2 + \left(\frac{\sigma_s}{S_{max}}\right)^2 = 1 \tag{16}$$

Where N_{max}, T_{max} and S_{max} represent the maximum values of the nominal stress components σ_n,σ_t and σ_s respectively. The complete failure in cohesive elements is found when (linear crit.):

$$\left(\frac{G_I}{G_{Ic}}\right) + \left(\frac{G_{II}}{G_{IIc}}\right) + \left(\frac{G_{III}}{G_{IIIc}}\right) = 1 \tag{17}$$

where G_j (with j=I,II,III) is the Energy Release Rate associated to the fracture mode j and G_{jc} is the critical Energy Release Rate associated to the fracture mode j. The stiffness K_n, characterizing the initial damage phase, can be determined from the transversal stiffness E_n of delaminated elements by considering the thickness of the cohesive element h_{eff} as shown in Fig. 2b. Therefore the cohesive stiffness in the normal direction is $K_{nn} = \frac{E_2}{h_{eff}}$, while the

cohesive stiffness in the first and in the second shear direction is $K_{ss} = K_{tt} = \frac{G}{h_{eff}}$. The area under the traction-separation curves is given by the fracture critical energy release rates, generally available in literature ($G_{Ic}, G_{IIc}, G_{IIIc}$).

3.3 Impact Test Modelling

The geometrical description and the boundary conditions of tested specimens is shown in Fig. 3, while the properties of the adopted material system (G1157\RTM-6) are shown in Table 2.

In Fig. 4 an exploded view of the adopted finite element model is presented.

Figure 5a shows that the positioning of cohesive elements between solid plies can be chosen according to three different modelling strategy.

The first modelling strategy uses coincident meshes for cohesive and solid elements with merged coincident nodes, resulting in less computational expensive analyses. According to the second strategy, "tie-constraints" contacts are used to link the non-coincident meshes of solid and cohesive elements. The chance to use different sizes for solid and cohesive elements allows to refine the cohesive element layers in order to obtain more accurate predictions of the

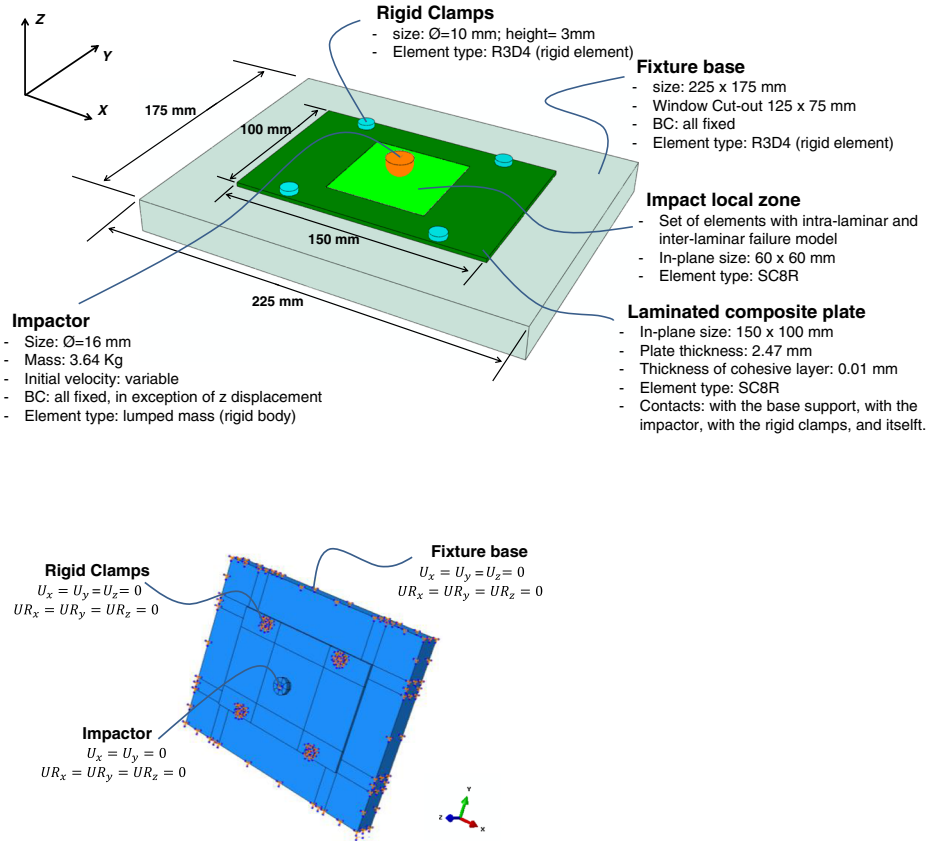

Fig. 3 Geometrical description of the impacted specimens and fixtures and boundary condition applied to the numerical model

Table 2 Material properties - G1157\RTM-6

Properties	Value
Density **Kg/m**^{3}	1400
Orthotropic properties	$E_{11} = 130050\,\text{MPa}$; $E_{22} = E_{33} = 11550\,\text{MPa}$
	$G_{12} = G_{13} = G_{23} = 6000\,\text{Mpa}$;
	$\nu_{12} = \nu_{13} = \nu_{23} = 0.312$
Strength	$X_T = 1460.7$; $X_C = 876.42$; $Y_T = 77.1145$; $Y_C = 241.435$
	$S_{12} = S_{13} = 90$; $S_{23} = 40$
In-plane fracture energies	$GF_{ft_C} = 16.4kJ/m^2$; $GF_{fc_C} = 5.9kJ/m^2$; $GF_{mt_c} = 0.5kJ/m^2$; $GF_{mc_C} = 4.62kJ/m^2$
Inter-laminar fracture toughness	G_{IC}=0.18kJ/m^2;G_{IIC}0.5kJ/m^2;G_{IIIC}=0.5kJ/m^2

delamination shape without increasing the number of solid elements leading to a substantial saving of computational cost. In this paper, the positioning of cohesive elements between solid plies has been performed according to the second modelling strategy as it has been shown in Fig. 4, where also the introduced "Global–local technique" [64, 65] can be appreciated. Despite of the relatively coarser mesh used for the supports and for the laminate boundaries, a very refined (with solid elements for each layer) has been adopted for the impacted area, in order to obtain a realistic simulation of the impact event. The refined area has been linked to global area through "tie constraints" (see Fig. 5b) with a "node to surface" tie formulation. For the impactor, rigid elements (R3D4), available from the Abaqus library, have been used.

4 Experimental Data and Simulation Results Correlation and Discussion

In this section experimental outputs and simulation results are correlated for the three investigated impact energy levels. The FE model results allow to understand the onset of the damage at ply level and to easily distinguish among the several failure mechanisms involved in

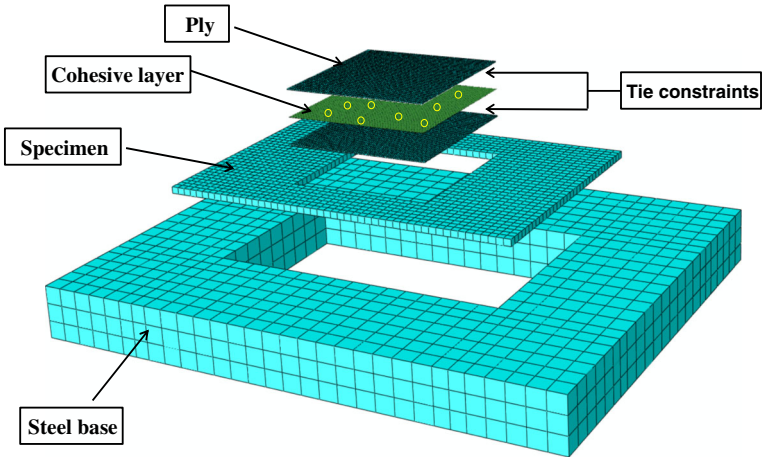

Fig. 4 Exploded view of the FE model

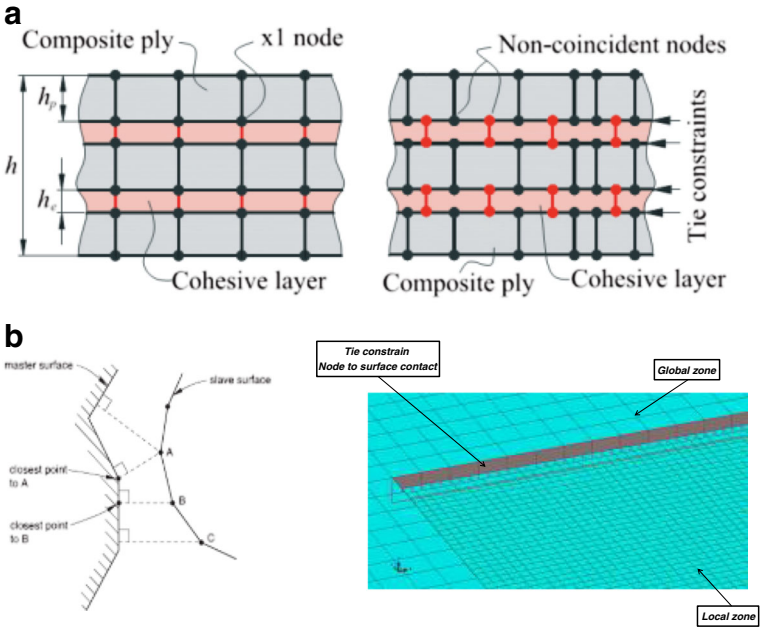

Fig. 5 **a** Cohesive modelling techniques; **b** Tie constraint between global and local zone

the impact event. The non-destructive testing outputs, presenting the damage status at the end of the impact tests, are integrated with the numerical results in order to investigate possible correlations between the final damage status and the damage formation at ply level, providing, at the same time, a validation of the adopted numerical tools. The impact energy values investigated in this paper (6, 10 and 13 J) have been simulated by changing the velocity of the impactor without varying its mass. In Fig. 6a, a representative view of the numerical out of plane displacements for an impact energy of 10 J is presented, showing the delaminations formation under the impact loading.

In Fig. 6b, the numerical results, in terms of deformed shapes and intra-laminar matrix damage formation, for a 10 J impact energy, are shown (these results give a suitable representation of the deformed shapes obtained also for the other impact energy levels). According to Fig. 6b, at 0.7 ms, the impactor comes into contact with the plate while, at 1.2 ms, the plate bends causing matrix cracking and small delaminations. Delaminations propagate, from 3.3 to 8.5 ms, to their final shapes leading to the full development of the impact damage. It is clear that the damage starts developing on the opposite side respect to the impact surface and progressively extends, during the impact event, towards the impact surface and along the laminate plane.

In Fig. 7, it is possible to appreciate the delaminations (painted in red in the cohesive interfaces), resulting mainly from the bending induced shears stress distribution around the impact area, in the lowest two plies interfaces opposed to the impact surface, for the three analysed impact energies. The most significant delaminations, for all the three analysed configurations, occurs at the lower interface, developing mainly along the direction of the lower 0° oriented plies. The size of the induced delaminations, as expected, increases with the impact energy. In Fig. 7, the matrix cracks created by the flexural in-plane stresses can also be

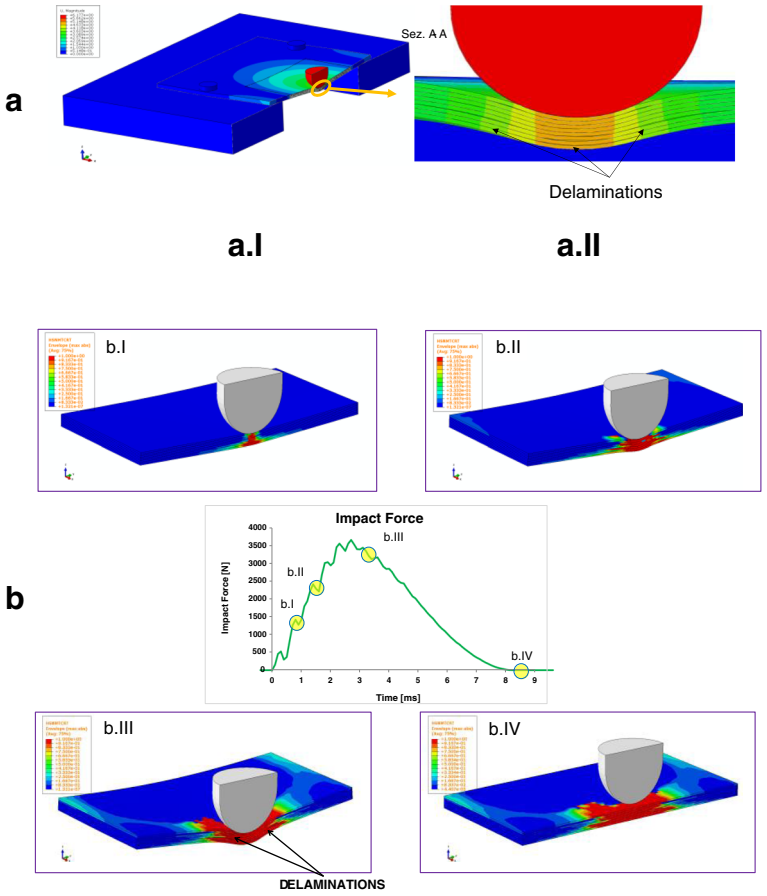

Fig. 6 **a** Out of plane displacements distribution during impact (10 J impact energy): *a.I*) sectioned full model; *a.II*) detail of the impact area; **b** Numerically predicted matrix cracking contours and delaminations for a 10 J energy impact - (*b.I*) 0.7 ms, (*b.II*) 1.2 ms, (*b.III*) 3.3 ms, and (*b.IV*) 8.5 ms

evaluated for the lowest three plies opposed to the impact surface. The status of the elements in these plies is reported (red = elements with complete matrix breakage; blue = pristine elements; green = elements with partially degraded matrix). For all the three impact energy levels the matrix damage seems to be almost equally distributed in the last three plies showing in the bottom ply a slightly more extended damaged area. The matrix cracking is clearly distributed along the fibres direction in each ply. The amount of the intra-laminar damaged area, as expected, increases with the impact energy. As previously remarked, three non-destructive testing techniques have been used to detect the damage induced by the impact event: thermography, ultrasonic A-scan and ultrasonic C-scan.

In Fig. 8, a comparison among all the NDT techniques output and the numerical results, in terms of impact induced delaminations' envelops length and width, is presented, for the three analysed impact energy levels. An overall good agreement between the numerical and the experimental delaminations' envelope sizes can be appreciated for all the experimental non-destructive techniques and for all the impact energy levels as summarised in Table 3.

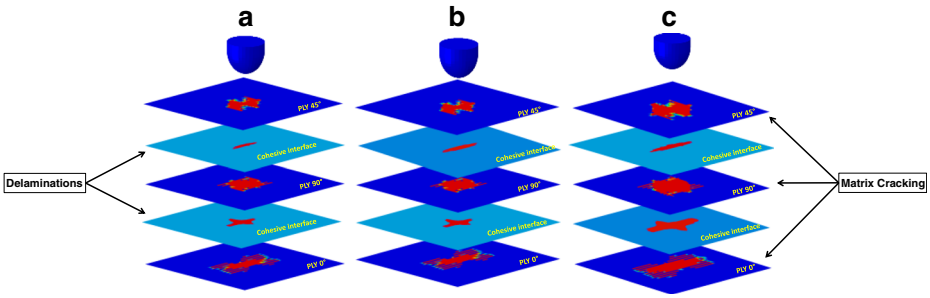

Fig. 7 Delaminations shapes and matrix cracking damage in the lower plies and intefaces – **a** 6 J impact energy; **b** 10 J impact energy and **c** 13 J impact energy

In Fig. 9, in order to better show the excellent correlation between the numerically determined delaminations and the experimental data, the numerical delaminations envelope outline (red dashed line) has been superimposed on Infrared thermography images for the three investigated impact energy levels. A slight numerical underestimation of the delaminated area can be observed when increasing the impact energy.

Indeed, almost all the experimental data seems to be in a reasonably good agreement each other and with the numerical results.

In Fig. 10a the impact force vs time curves are presented for the three impact energy levels. The good agreement between the numerical and experimental curves can be easily appreciated up to the peak force which is slightly underestimated. During the unloading phase the numerical data deviate from the experimental ones probably due to the overestimation of the impact induced damage. On the other hand, due to the very good agreement with the experimental data observed for inter-laminar damage, it could be assumed that the

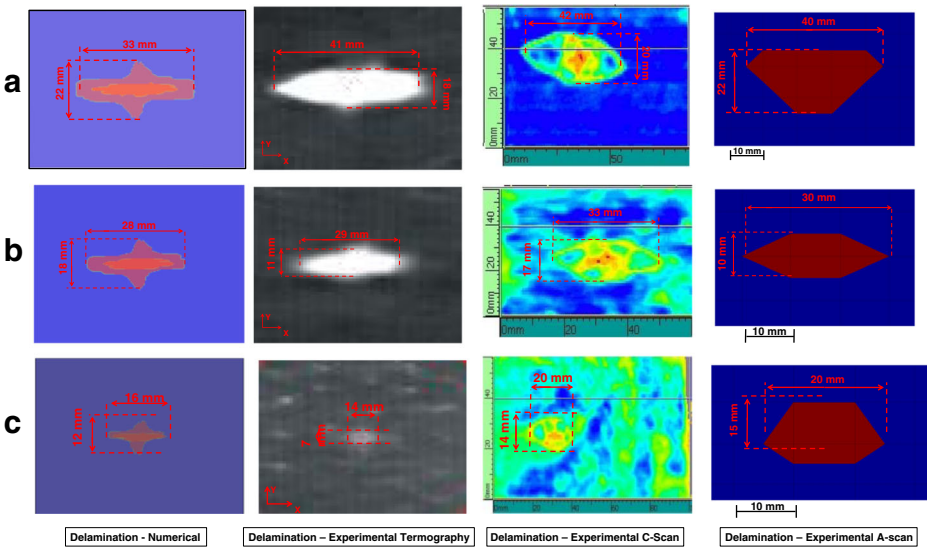

Fig. 8 NDT data and numerical result comparisons in term of delaminations' envelope: **a** 13 J impact energy; **b** 10 J impact energy; **c** 6 J impact energy

Table 3 Delaminations' envelope dimensions - comparisons between experimental data and numerical results

		Thermography	Ultrasonic A-scan	Ultrasonic C-scan	Numerical
6 J	Length	14 mm	20 mm	20 mm	16 mm
	Width	7 mm	15 mm	14 mm	12 mm
10 J	Length	29 mm	30 mm	33 mm	28 mm
	Width	11 mm	10 mm	17 mm	18 mm
13 J	Length	41 mm	40 mm	42 mm	33 mm
	Width	18 mm	22 mm	20 mm	22 mm

overestimation of the damage could be related mainly to the intra-laminar damage (breakage of the fiber and matrix). This overestimation is reduced for higher impact energy levels.

For the three investigated impact energy values (6, 10 and 13 J) the force-displacement curves have been reported in Fig. 10b. The numerical results are very satisfactory for the impact simulation at 13 J where both the impact and the unloading phases are very well predicted, while for lower impact energy levels the unloading phase seems to be not correctly simulated. This behaviour can be related to the aforementioned possible overestimation of the induced intra-laminar damage for the lower impact energy levels. In general, for all the investigated impact energy levels, the proposed finite element model, has been found effective and accurate in predicting the final inter-laminar damage status, as demonstrated by the very good agreement between numerical results and NDT measurements. A probable overestimation of the induced intra-laminar damage, for low impact energy levels, causes a slight deviation from the experimental readings, in terms of impact force and induced displacements, in the unloading phase.

5 Conclusions

The integrated numerical-experimental approach, presented in this paper, has been found able to provide interesting information on the inter-laminar damage formation and evolution in composite plates under low velocity impacts. Indeed three different non-destructive testing (NDT) techniques have been used to characterise the final damage induced by low velocity impacts on the analysed composite plates. In conjunction with the experimental activity, a sophisticated numerical model has been used to investigate the onset and the evolution of the intra-laminar and inter-laminar damage during the impact event. The finite element model

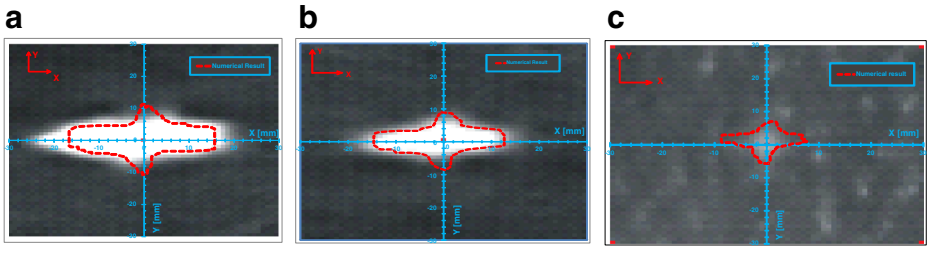

Fig. 9 Thermography NDT and numerical delaminations' envelope: **a** 13 J impact energy; **b** 10 J impact energy; **c** 6 J impact energy

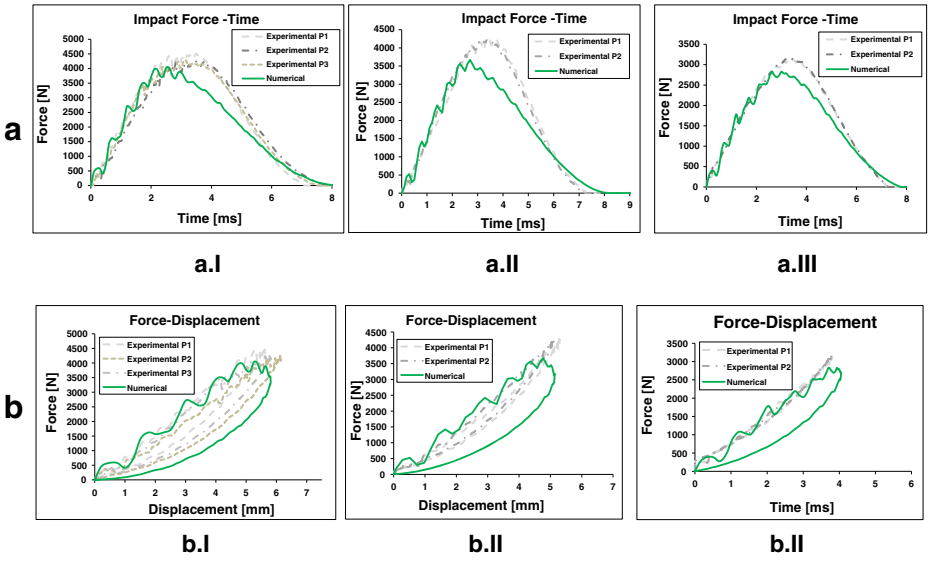

Fig. 10 **a** Comparison between numerical and experimental Force-time curves: *a.I*) 13 J impact energy, *a.II*) 10 J impact energy, *a.III*) 6 J impact energy; **b** Comparison between numerical and experimental force-displacements curve: *b.I*) 13 J impact energy; *b.II*) 10 J impact energy; *b.III*) 6 J impact energy

proposed, able to predict both inter-laminar and intra-laminar damages in the composite plate arising as a consequence of the bending induced by the impactor, has been found effective and accurate in predicting the final inter-laminar damage status. Indeed the comparison in terms of delaminations envelope size between numerical results and experimental data has been found excellent for all the investigated impact energy levels. For instance all the adopted NDI techniques (infrared thermography, ultrasonic C-Scan and A-scan) have provided data, in terms of delamination envelope shape and size, in very good agreement each other, for all the investigated impact energy levels. As demonstrated by the comparisons between experimental data and numerical results, in terms of impact force and displacements curves, the proposed numerical tool seems to slightly overestimate the impact induced damage. This overestimation, probably related to the intra-laminar damage, is appreciable especially for lower impact energy levels. However, even with these limitations, the numerical tool has been found able to fit the experimental activity providing reasonable interpretations of the induce inter-laminar damage onset and evolution at ply level in agreement with the final damage status observed experimentally.

References

1. Abrate, S.: Impact on Composite Structures. Cambridge University Press, Cambridge (1998)
2. Reid, S., Zhou, G.: Impact Behaviour of Fibre-reinforced Composite Materials and Structures. CRC Press, Cambridge (2000)
3. Varas, D., Artero-Guerrero, J., Pernas-Sánchez, J., López-Puente, J.: Analysis of high velocity impacts of steel cylinders on thin carbon/epoxy woven laminates. Compos. Struct. **95**, 623–629 (2013)
4. Artero-Guerrero, J., Pernas-Sánchez, J., Varas, D., López-Puente, J.: Numerical analysis of CFRP fluid-filled tubes subjected to high-velocity impact. Compos. Struct. **96**, 286–297 (2013)

5. Riccio, A., Di Felice, G., Saputo, S., Scaramuzzino, F.: A numerical study on low velocity impact induced damage in stiffened composite panels. J. Comput. Simul. Model. **3**(1), 044–047 (2013)
6. Caputo, F., Di Gennaro, F., Lamanna, G., Lefons, A., Riccio, A.: Numerical procedures for damage mechanisms analysis in CFRP composites. Key Eng. Mater. **569–570**, 111–118 (2013)
7. Soutis, C., Curtis, P.T.: Prediction of the post-impact compressive strength of CFRP laminated composites. Compos. Sci. Technol. **56**, 677–684 (1996)
8. Wisnom, M.R.: The role of delamination in failure of fibre-reinforced composites. Philos. Trans. R. Soc. A Math. Phys. Eng. Sci. **370**(1965), 1850–1870 (2012)
9. Abrate, S.: Modeling of impacts on composite structures. Compos. Struct. **51**, 129–138 (2001)
10. Feraboli, P., Kedward, K.T.: A new composite structure impact performance assessment program. Compos. Sci. Technol. **66**, 1336–1347 (2006)
11. Lopes, C.S., Seresta, O., Coquet, Y., Gnrdal, Z., Camanho, P.P., Thuis, B.: Low-velocity impact damage on dispersed stacking sequence laminates. Part I: experiments. Compos. Sci. Technol. **69**, 926–936 (2009)
12. Tita, V., de Carvalho, J., Vandepitte, D.: Failure analysis of low velocity impact on thin composite laminates: experimental and numerical approaches. Compos. Struct. **83**, 413–428 (2008)
13. Aktas, M., Atas, C., Is_ten, B.M., Karakuzu, R.: An experimental investigation of the impact response of composite laminates. Compos. Struct. **87**, 307–313 (2009)
14. Li, C., Hu, N., Yin, Y., Sekine, H., Fukunaga, H.: Low-velocity impact-induced damage of continuous fiber-reinforced composite laminates. Part I. An FEM numerical model. Compos. Part A **33**, 1055–1062 (2002)
15. González, E.V., Maimí, P., Camanho, P.P., Turon, A., Mayugo, J.A.: Simulation of dropweight impact and compression after impact tests on composite laminates. Compos. Struct. **94**(11), 3364–3378 (2012)
16. Riccio, A., Raimondo, A., Fragale, S., Camerlingo, F., Gambino, B., Toscano, C., Tescione, D.: Delaminations buckling and growth phenomena in stiffened composite panels under compression. Part I: an Experimental Study. J. Compos. Mater. (2013). doi:10.1177/0021998313502741
17. Riccio, A., Raimondo, A., Di Caprio, F., Scaramuzzino, F.: Delaminations buckling and growth phenomena in stiffened composite panels under compression. Part II: a Numerical Study. J. Compos. Mater. (2013). doi:10.1177/0021998313502742
18. Choi, I.H.: Low-velocity impact analysis of composite laminates under initial inplane load. Compos. Struct. **86**, 251–257 (2008) [Fourteenth International Conference on Composite Structures (ICCS/14)]
19. Olsson, R.: Analytical prediction of large mass impact damage in composite laminates. Compos. Part A **32**, 1207–1215 (2001)
20. Olsson, R., Donadon, M.V., Falzon, B.G.: Delamination threshold load for dynamic impact on plates. Int. J. Solids Struct. **43**, 3124–3141 (2006)
21. Elder, D.J., Thomson, R.S., Nguyen, M.W., Scott, M.L.: Review of delamination predictive methods for low speed impact of composite laminates. Compos. Struct. **66**, 677–683 (2004)
22. Riccio, A., Raimondo, A., Borrelli, R., Mercurio, U., Tescione, D., Scaramuzzino, F.: Numerical simulations of inter-laminar damage evolution in a composite wing box. Appl. Compos. Mater. (2013). doi:10.1007/s10443-013-9347-2
23. Pietropaoli, E., Riccio, A.: Finite element analysis of the stability (buckling and post- buckling) of composite laminated structures: well established procedures and challenges. Appl. Compos. Mater. **19**, 79–96 (2012)
24. Allix, O., Ladeveze, P., Corigliano, A.: Damage analysis of interlaminar fracture specimens. Compos. Struct. **31**(1), 61–74 (1995)
25. Tay, T.E., Liu, G., Tan, V.B.C., Sun, X.S., Pham, D.C.: Progressive failure analysis of composites. J. Compos. Mater. **42**(18), 1921–1964 (2008)
26. Wisnom, M.R.: Modelling discrete failures in composites with interface elements. Compos. A: Appl. Sci. Manuf. **41**(7), 795–805 (2010)
27. Riccio, A., Scaramuzzino, F., Perugini, P.: Influence of contact phenomena on embedded delamination growth in composites. AIAA J. **41**(5), 933–940 (2003)
28. Riccio, A., Raimondo, A., Scaramuzzino, F.: Skin stringer debonding evolution in stiffened composites under compressive load: a novel numerical approach. Key Eng. Mater. **577–578**, 605–608 (2014)
29. Riccio, A., Raimondo, A., Scaramuzzino, F.: A study on skin delaminations growth in stiffened composite panels by a novel numerical approach. Appl. Compos. Mater. **20**(4), 465–488 (2013)
30. Tay, T.E.: Characterization and analysis of delamination fracture in composites: an overview of developments from 1990 to 2001. Appl. Mech. Rev. **56**(1), 1–32 (2003)
31. Camanho, P.P., Davila, C.G., De Moura, M.F.: Numerical simulation of mixed-mode progressive delamination in composite materials. J. Compos. Mater. **37**(16), 1415–1438 (2003)
32. Wang, Y., Williams, J.G.: Corrections for mode II fracture toughness specimens of composites materials. Compos. Sci. Technol. **43**, 251–256 (1992)

33. Suemasu, H.: An experimental method to measure the mode-III inter-laminar fracture toughness of composite laminates. Compos. Sci. Technol. **59**, 1015–1021 (1999)
34. Pietropaoli, E., Riccio, A.: Formulation and assessment of an enhanced finite element procedure for the analysis of delamination growth phenomena in composite structures. Compos. Sci. Technol. **71**(6), 836–846 (2011)
35. Aymerich, F., Dore, F., Priolo, P.: Simulation of multiple delaminations in impacted cross-ply laminates using a finite element model based on cohesive interface elements. Compos. Sci. Technol. **69**, 1699–1709 (2009)
36. Amaro, A.M., Santos, J.B., Cirne, J.S.: Delamination depth in composites laminates with interface elements and ultrasound analysis. Strain **47**(2), 138–145 (2011)
37. Pietropaoli, E., Riccio, A.: On the robustness of finite element procedures based on Virtual Crack Closure Technique and fail release approach for delamination growth phenomena. Definition and assessment of a novel methodology. Compos. Sci. Technol. **70**(8), 1288–1300 (2010)
38. Bouvet, C., Rivallant, S., Barrau, J.J.: Low velocity impact modeling in composite laminates capturing permanent indentation. Compos. Sci. Technol. **72**(16), 1977–1988 (2012)
39. De Moura, M.F.S.F., Gonçalves, J.P.M.: Modelling the interaction between matrix cracking and delamination in carbon–epoxy laminates under low velocity impact. Compos. Sci. Technol. **64**(7), 1021–1027 (2004)
40. Zhang, Y., Zhu, P., Lai, X.: Finite element analysis of low-velocity impact damage in composite laminated plates. Mater. Des. **27**(6), 513–519 (2006)
41. Aoki, Y., Suemasu, H., Ishikawa, T.: Damage propagation in CFRP laminates subjected to low velocity impact and static indentation. Adv. Compos. Mater. **16**(1), 45–61 (2007)
42. Aymerich, F., Dore, F., Priolo, P.: Prediction of impact-induced delamination in cross-ply composite laminates using cohesive interface elements. Compos. Sci. Technol. **68**(12), 2383–2390 (2008)
43. Bouvet, C., Castanié, B., Bizeul, M., Barrau, J.J.: Low velocity impact modelling in laminate composite panels with discrete interface elements. Int. J. Solids Struct. **46**, 2809–2821 (2009)
44. Bouvet, C., Hongkarnjanakul, N., Rivallant, S., Barrau, J.J.: Discrete impact modeling of inter- and intra-laminar failure in composites. In: Abrate, S., Castanié, B., Rajapakse, Y.D.S. (eds.) Dynamic Failure of Composite and Sandwich Structures, pp. 339–392. Springer, Dordrecht (2013)
45. De Borst, Remmers, J.J., Needleman, A.: Mesh-independent discrete numerical representations of cohesive-zone models. Eng. Fract. Mech. **73**(2), 160–177 (2006)
46. Iannucci, L.: Progressive failure modelling of woven carbon composite under impact. Int. J. Impact Eng. **32**(6), 1013–1043 (2006)
47. Maimí, P., Camanho, P.P., Mayugo, J.A., Dávila, C.G.: A continuum damage model for composite laminates: part I—constitutive model. Mech. Mater. **39**, 897–908 (2007)
48. Donadon, M.V., Iannucci, L., Falzon, B.G., Hodgkinson, J.M., de Almeida, S.F.M.: A progressive failure model for composite laminates subjected to low velocity impact damage. Comput. Struct. **86**, 1232–1252 (2008)
49. Maimí, P., Mayugo, J.A., Camanho, P.P.: A three-dimensional damage model for transversely isotropic composite laminates. J. Compos. Mater. **42**(25), 2717–2745 (2008)
50. Falzon, B.G., Apruzzese, P.: Numerical analysis of intralaminar failure mechanisms in composite structures. Part I: FE implementation. Compos. Struct. **93**, 1039–1046 (2011)
51. Falzon, B.G., Apruzzese, P.: Numerical analysis of intralaminar failure mechanisms in composite structures. Part II: applications. Compos. Struct. **93**, 1047–1053 (2011)
52. Garnich, M.R., Akula, V.M.K.: Review of degradation models for progressive failure analysis of fiber reinforced polymer composites. Appl. Mech. Rev. **62**(1), 1–33 (2009)
53. Riccio, A., Di Felice, G., Saputo, S., Scaramuzzino, F.: Stacking sequence effects on damage onset in composite laminate subjected to low velocity impact. Procedia Eng. **88**(1), 222–229 (2014)
54. Lopes, C.S., Camanho, P.P., Gürdal, Z., Maimí, P., González, E.V.: Low-velocity impact damage on dispersed stacking sequence laminates. Part II: numerical simulations. Compos. Sci. Technol. **69**, 937–947 (2009)
55. Faggiani, A., Falzon, B.G.: Predicting low-velocity impact damage on a stiffened composite panel. Compos. A: Appl. Sci. Manuf. **41**, 737–749 (2010)
56. Shi, Y., Swait, T., Soutis, C.: Modelling damage evolution in composite laminates subjected to low velocity impact. Compos. Struct. **94**(9), 2902–2913 (2012)
57. ABAQUS Analysis user's manual 6.11 (2011)
58. Hashin, Z., Rotem, A.: A fatigue criterion for fiber -reinforced materials. J. Compos. Mater. **7**, 448–464 (1973)
59. Hashin, Z.: Failure criteria for unidirectional fiber composites. J. Appl. Mech. **47**, 329–334 (1980)
60. Camanho, P.P., Davila, C.G.: Mixed-mode decohesion finite elements for the simulation of delamination in composite materials. NASA/TM-2002–211737, pp. 1–37. (2002)
61. Bazant, Z.P., Oh, B.H.: Crack band theory for fracture of concrete. Mater. Struct. **16**, 155–177 (1983)

62. Lapczyk, I., Hurtado, J.A.: Progressive damage modeling in fiber-reinforced materials. Compos. A: Appl. Sci. Manuf. **38**(11), 2333–2341 (2007)
63. Toscano, C., Riccio, A., Camerlingo, F., Meola, C.: On the use of lockin thermography to monitor delamination growth in composite panels under compression. Sci. Eng. Compos. Mater. (2013). doi:10.1515/secm-2013-0156
64. Pietropaoli, E., Riccio, A.: A global/local finite element approach for predicting interlaminar and intralaminar damage evolution in composite stiffened panels under compressive load. Appl. Compos. Mater. **18**(2), 113–125 (2011)
65. Riccio, A., Di Felice, G., LaManna, G., Antonucci, V., Caputo, F., Lopresto, V., Zarrelli, M.: A global-local numerical model for the prediction of impact induced damage in composite laminates. Appl. Compos. Mater. (2013). doi:10.1007/s10443-013-9343-6